Comparative structural stiffness: Exploiting 3D-printing

Lawrence N. Virgin[a)]
Department of Mechanical Engineering and Material Science, Duke University, Durham, North Carolina 27708-0300

(Received 24 March 2020; accepted 29 July 2020)

The teaching of structural stiffness is one of the keystones of the undergraduate curriculum in mechanics and the strength of materials. Standard linear theory, going back to Hooke's law, has proven to be very successful in predicting the performance of elastic structures under load. Many courses in basic mechanics have a conventional laboratory component often involving a universal testing machine and extensometer. However, the advent of 3D printing presents an appealing pedagogical opportunity mid-way between theory and a formal lab experience. The material contained in this paper focuses on using the 3D printing of relatively simple, flexible cantilever structures. The relatively high resolution of modern 3D printers facilitates the production of slender (elastically deformable) structures, and thus provides an opportunity to exploit geometric parametric variations to enhance a practical understanding of fundamental mechanics concepts such as stiffness. This approach has proved successful in initial inclusion in both the classroom via demonstration models, as well as in the lab in which elementary facilities can be utilized to acquire data. The boundary conditions associated with a cantilever, and the application of a point force are especially simple to produce in practice, and provide an effective tactile demonstration of the influence of geometrical changes on the relation between force and deflection, i.e., stiffness.
https://doi.org/10.1119/10.0001756

I. INTRODUCTION

The ability of structural elements, and structures in general, to effectively withstand load is often achieved by flexural elastic deformation and the storage of strain energy. Provided the resulting stresses and deflections are kept within reasonable limits, this is often the basis of an economic design (minimal material use). Very often there is a linear relation between load and deflection, at least for relatively small deflections, broadly in the range of practical application.[1] This is the case for beam theory, for example, and also allows an effective demonstration of the utility of using dimensionless variables.[2–4] Coupled with the versatility of 3D printers to conveniently produce structures with specific geometry, and in an elastic material, the teaching of solid mechanics can be enhanced by simple hands-on demonstration models, which can also be used to acquire data.[5]

3D printing has been introduced by a number of instructors to enhance the quality of instruction in a variety of contexts, including an appreciation of auxetic behavior,[6] laboratory modules,[7] mechanical behavior,[8,9] general mechanical systems,[10] and general education.[11] The primary focus of this paper is on flexural behavior of linear elastic elements, for which we invoke Hooke's law, $F = kx$, i.e., force F causes a proportionate deflection x, characterized by the stiffness of coefficient k. The elastic flexural stiffness of a simple structure (here, a cantilever) is assessed, primarily through a subjective, tactile appreciation, and the ways in which the stiffness changes with geometry.[12,13]

The key mechanism in this paper is a comparison based on parameter variation. Thus, the demonstration models can be used based purely on feel, where simply pushing down on the ends of cantilevers sequentially provides a direct assessment of stiffness. There is nothing unique about the dimensions chosen here, and students and instructors are encouraged to produce their own geometries. If measurements are made, then the results can be conveniently presented in terms of dimensionless quantities.

We shall focus on five fundamental cases, in which a change in geometry leads to a change in stiffness. Since the 3D-printed specimens are all produced monolithically using the same material, we isolate a specific parameter, so that the effect on stiffness can be appreciated in a comparative sense. We shall focus on sets of tip-loaded cantilevers (see Fig. 1), and specifically, we consider the following:

- a simple cantilever, under variation of length: Fig. 1(a);
- a simple cantilever, under variation of width: Fig. 1(b);
- a cantilever with different linearly tapered widths: Fig. 1(c);
- a cantilever with a longitudinal stiffener (rib) of varying depth: Fig. 1(d); and
- a cantilever with a turnaround section with varying length: Fig. 1(e).

All of these cantilever sets can be printed with relative ease using any 3D-printer (STL files are available from the author by request). We use the linear relation between force and deflection at the free end as a measure of stiffness.

In the classroom setting, students are in a position to assess stiffness by, for example, pushing down on each cantilever sequentially and experiencing the resistance, and then feeling the differences between each member of a cantilever set. In this way, they can verify how this stiffness depends on the change in geometry according to theory.

II. BACKGROUND BEAM THEORY

The general equation of the elastic curve relates the lateral deformation (y) of a beam along its length x to its geometry and loading,[1]

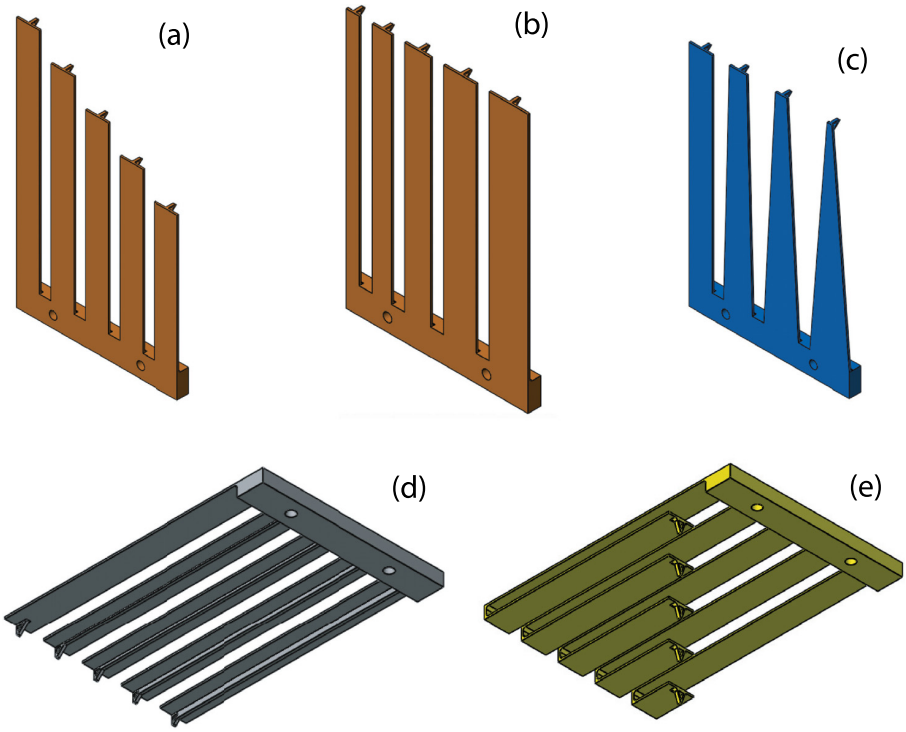

Fig. 1. Isometric views of the 3D-printed cantilever sets: (a) variable length, (b) variable width, and (c) variable taper. Views from below: (d) cantilevers with variable ribs and (e) cantilevers with variable length turnarounds. A small eye is printed at the tip to facilitate weight attachment.

$$EI\frac{d^2y}{dx^2} = M, \tag{1}$$

in which M is the applied bending moment (that depends on external loading and boundary conditions), EI is the flexural rigidity, with Young's modulus E and second moment of area I. Equation (1) is based on a number of assumptions, including linear elastic material, thin (slender) geometry, and is restricted to relatively small deflections (for example, the curvature expression d^2y/dx^2 is approximate). It is widely used (often referred to as Euler–Bernoulli theory), it can be used to estimate Young's modulus,[14] and is easily extended to include vibrations (see Appendix B). We are specifically interested in cantilevers with boundary conditions supplying zero deflection and slope at the built-in, clamped end. The coordinate system and notation for our cantilevers are shown in Fig. 2.

III. A SIMPLE CANTILEVER

One of the simplest cases is a cantilever beam of rectangular cross section subject to a lateral tip load. Assuming a constant (prismatic) cross section of breadth b, thickness d, (the second moment of area is $b \times d^3/12$ for a rectangle), length L, clamped at $x = L$ and subject to a (downwards) point load F at $x = 0$ (see Fig. 2(a)), we have the governing equation

$$EI\frac{d^2y}{dx^2} = -Fx, \tag{2}$$

which can be integrated twice, and using the boundary conditions at the clamped (right hand) end B, $(y(L) = y'(L) = 0)$, gives a deflected shape

$$y = \frac{FL^3}{3EI}\left[-1 + \frac{3}{2}\left(\frac{x}{L}\right) - \frac{1}{2}\left(\frac{x}{L}\right)^3\right]. \tag{3}$$

We immediately see the linear relation between F and y. At the free end A, $x = 0$, we obtain the tip deflection $y_{tip} = -FL^3/3EI$, thus a stiffness of $k = 3EI/L^3$. It is the relation between k and geometry that is the focus of this study.

In general, we shall examine the effect of systematically varying parameters away from a standard baseline geometry, as outlined in Table I. These values are generally used for nondimensionalization in later figures, i.e., parameters are typically divided by a baseline value and indicated by an over-bar. Furthermore, E is typically a little lower than 2.1 GPa (the reference value) due to the 3D-printing process.[9] However, we are primarily interested in how geometrical changes influence stiffness in a relative sense with all cantilevers printed with the same thickness and using the same (ABS thermoplastic) material. Small weights were attached to the ends of the cantilevers resulting in vertical deflection. The deflections included later were generally measured using a proximity sensor, with an accuracy of about 1/40 mm. The Appendix includes some results based on a more sophisticated experimental approach (for example using a load cell), but in general, we simply observe how the cantilevers deflect under load, and this is tantamount to feeling the resistance to pushing on each cantilever by hand.

As introductory examples, we will examine the effect of varying the width b and the length L. We subject the end to the same specific vertical load (a weight), whereas more formally (in a lab setting), the stiffness is characterized by how force and deflection are related over a range, with the slope of a linear fit providing an accurate estimate of stiffness.

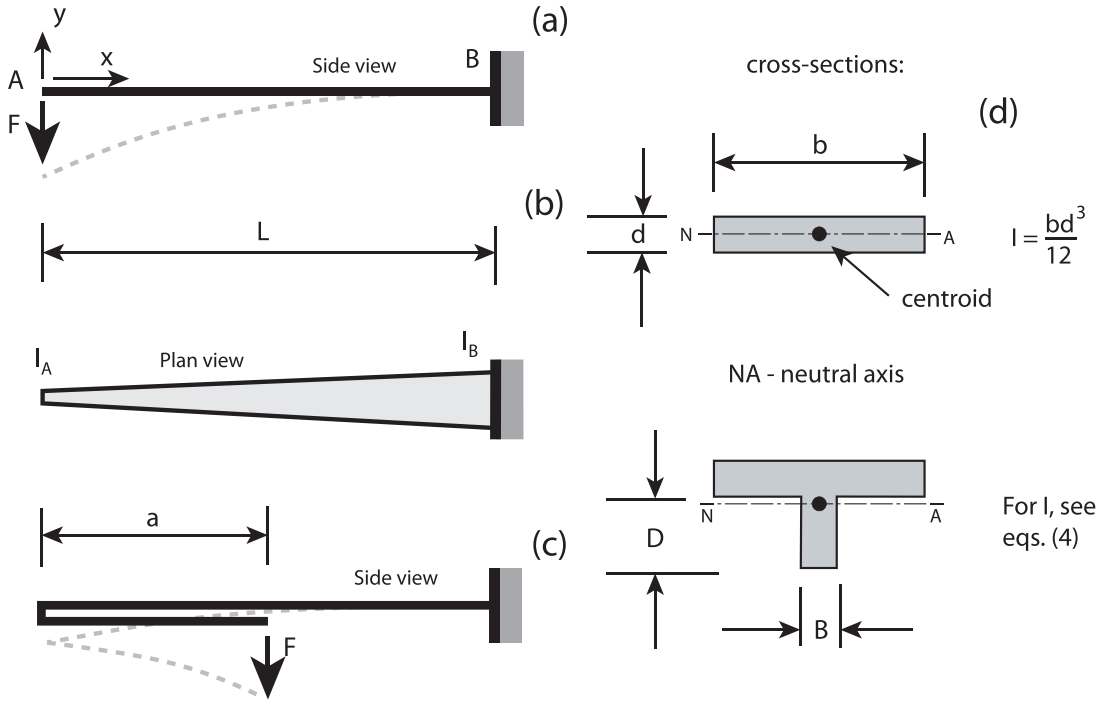

Fig. 2. The geometry of a cantilever: (a) the standard case, (b) a tapered cantilever, (c) a cantilever with a turnaround, and (d) cross-sectional shapes, including a rib stiffener in which the extra material shifts the centroid and neutral axis (increasing I).

Figures 3 and 4 shows the effect of varying these two parameters in terms of tip deflection and stiffness, including some photographic images. Here, the relations are normalized with respect to the aforementioned standard cantilever (indicated by the black circles in subsequent plots). In dimensional terms, we use $L = 120, 140, 160, 180, 200$ mm and $b = 10, 15, 20, 25, 30$ mm, with the specific cases indicated by the open circles points for experimental data in this, and later figures. The Appendix contains a detailed measured example for two different lengths under variable load, together with tabulated values corresponding to the datapoints shown in the figures. These parameter dependencies also underlie the notion of propagation of uncertainty and measurement error. For example, the thickness and stiffness are related cubically and hence any error in measuring the thickness (which is generally small) has a tendency to be propagated to a greater extent than say, the width, although this issue will not be addressed here.[15,16]

Table I. The standard cantilever configuration, providing a baseline stiffness, about which parameter variations are taken. That is, this specific geometry typically appears in the middle of each printed set.

Length, L	180 mm
Width, b	20 mm
Thickness[a], d	1.68 mm
Second moment of area[b], I	7.9 mm^4
Young's modulus, E	2.1 GPa
Stiffness, k	8.54 N/m
Mass applied to the tip, i.e., load, F = mg → deflection, y_0	29 g, 0.285 N, ≈33 mm

[a]A careful measurement of thickness for the 3D-printed specimens to be described later, gave an average value $d = 1.68$ mm (compared to a prescribed thickness of 1.5 mm), a relatively precise parameter with an enhanced sensitivity due to its effect on the second moment of area, and the small dimension most sensitive to the resolution of the 3D-printer.
[b]In the weaker direction, and about the (horizontal) neutral axis passing through the centroid.

It is important to recall some of the limitations of standard beam theory, including the restriction to relatively small deflections. For example, the least wide cantilever (10 mm) deflects vertically about 70 mm at the tip when subject to an end mass of 29 g, and this corresponds to y_{tip}/L of about 35%, a value near the curvature limit of the linear theory.[1]

A. A note on self-weight

We also mention that there is a small deflection associated with self-weight, at least where the cantilevers are oriented horizontally. Using the same linear theory, and an evenly distributed load, leads to a tip deflection $y_{tip} = fL^4/8EI$, where f is the distributed load (per unit length).[12] The density of the material used (ABS thermoplastic) in this study is typically close to 1050 Kg/m^3, corresponding to "solid" print settings, although the density of prints can be adjusted. Thus, for example, the standard cantilever weighs about 6 g, leading to a tip deflection of approximately 2.7 mm, an order of magnitude smaller that the deflection of close to 40 mm under the 29 g end-weight (which we can choose to vary). In general, the weight scales with volume (bdL), whereas the stiffness scales as $(b(d/L)^3)$. Given the range of geometries and weights used in this study, self-weight is ignored. However, when assessing stiffness by hand, the models resist force about a natural equilibrium shape, and can also be "held" in a vertical orientation. Self-weight does provide an alternative opportunity to demonstrate comparative stiffness based on the "natural" shape of unloaded, relatively low

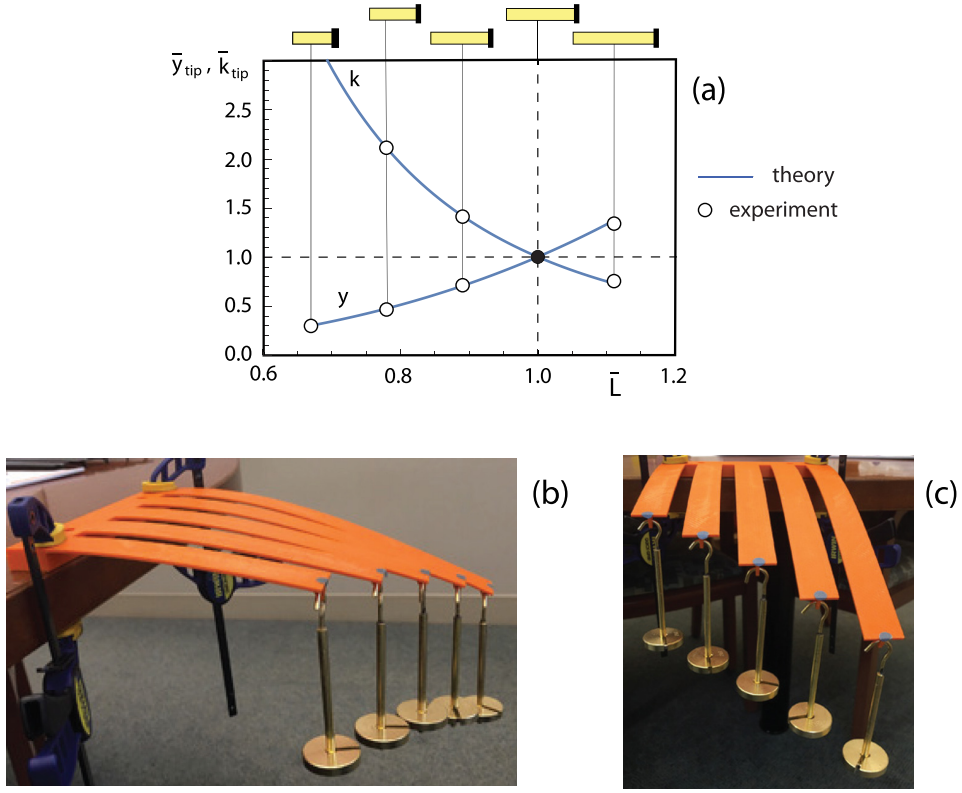

Fig. 3. (a) The effect of varying the length L on stiffness and hence the tip deflection, $\bar{y}_{tip} \equiv y_{tip}/y_0$, and (b) and (c) images of the cantilevers under the action of 29 g end-masses. In this and subsequent figures, the continuous lines and open circles are theory and experimental data, respectively.

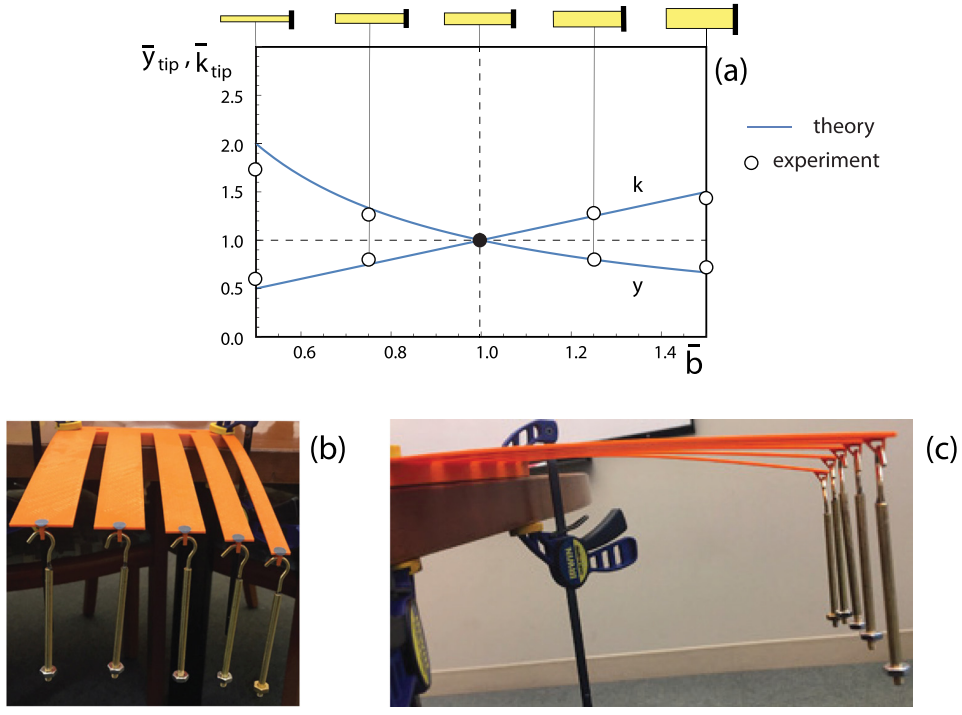

Fig. 4. (a) The effect of varying the width b on stiffness and hence the tip deflection, $\bar{y}_{tip} \equiv y_{tip}/y_0$, (b) image with 9 g end-masses, and (c) an alternative view of the cantilevers with 9 g end-masses (with proportionate deflections).

stiffness cantilevers allowed to droop when oriented horizontally (but not so much as to violate the linear theory). The vertical orientation is also natural for assessing natural frequency, rather like a tuning fork.[17]

IV. RIB-STIFFENED CANTILEVERS

The rectangular cross section provides a simple expression for the second moment of area: $I = bd^3/12$. A convenient way of increasing I is to effectively move the material further away from the neutral axis (that passes through the centroid) by adding a rib-stiffener, giving a T-section (also the reason why I-sections are effective in beams). This is shown schematically in part (d) of Fig. 2, in which we fix the rib width B at 2 mm and then systematically change the rib height, $D = 0, 1, 2, 3, 4$ mm. The general expressions for area A, centroid location (y_c), and second moment of area I, are readily available for typical shapes:[18]

$$\begin{aligned} A &= bd + DB, \\ y_c &= [(D + d/2)db + D^2B/2]/A, \\ I &= BD(y_c - D/2)^2 + BD^3/12 \\ &\quad + db(D + d/2 - y_c)^2 + d^3b/12. \end{aligned} \tag{4}$$

Again, we seek to observe the effect of adding the stiffening rib, and this is shown in Fig. 5 in which the second moment of area (and hence stiffness) increases with rib height. And again, the measured data corresponding to the 3D-printed specimens are indicated by the open circle data points, with the black data point corresponding to the baseline (rectangular cross section, no rib) case. The interesting part of this result is that the stiffness increases much faster than the area (and hence mass) with rib height. For example, relative to the no-rib standard case ($D = 0$), for a rib height of 3 mm, the area increases by 18%, whereas the second moment of area (and hence stiffness) increases by a little over 500%. Many components of aircraft structures (fuselage and wings) typically include panels with stiffeners/ribs, an application where weight-saving is paramount.

V. TAPERED CANTILEVERS

It is often the case that a cantilever is tapered, for example, a fishing rod, or tree, or the wing of an aircraft. Referring to Fig. 2(b), suppose we have a rectangular cross section with a width $b = b(x)$ that varies linearly such that we have a second moment of area I_A at the left end and I_B at the right, i.e., $I_x = I_A(1 + Kx/L)$, with $K = I_B/I_A - 1$. Again using the $180 \times 20 \times 1.68$ mm geometry as the baseline case, we consider a set of four cantilevers: $(b_A,\ b_B) = (20, 20), (15, 25), (10, 30), (5, 35)$ mm, see Fig. 2(b). An alternative approach would be to keep I_B constant, say 20 mm, and reduce I_A, resulting in a progressive reduction in stiffness. For example, if the baseline cantilever was tapered to 5 mm at the free end, we would obtain a stiffness reduction of about 20%. Given the relatively simple variation in $I = I(x)$, we can directly incorporate this expression when integrating Eq. (2), although this is not trivial. However, standard cases have been tabulated. For example, in Roark's formulas for stress

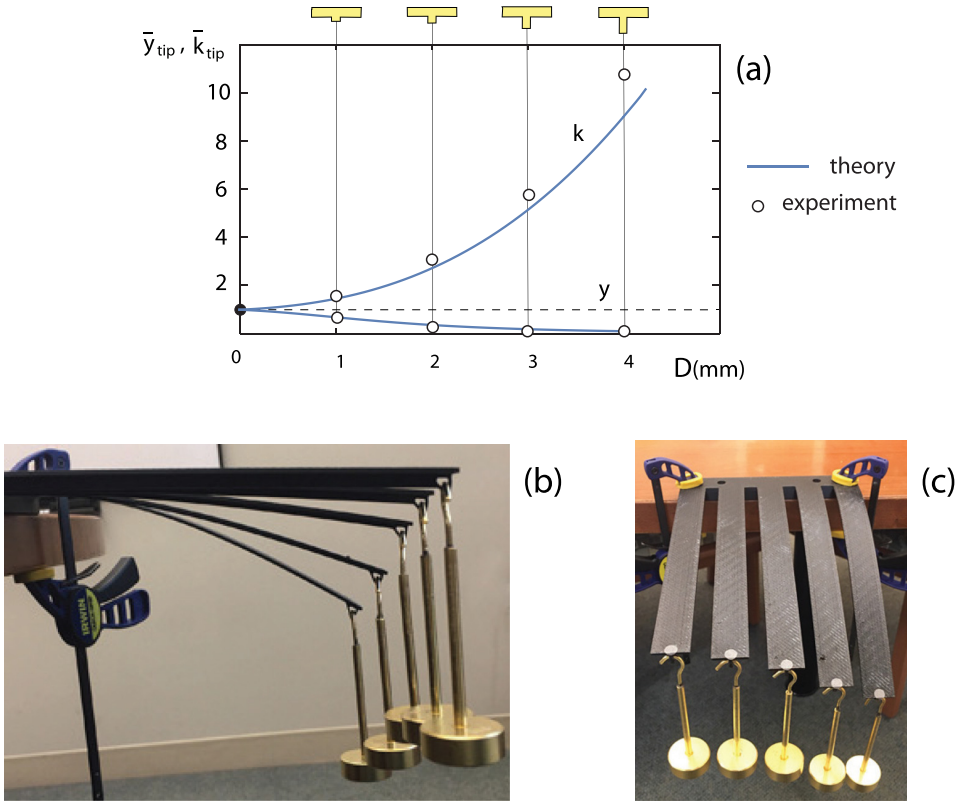

Fig. 5. (a) The effect of including a small rib on the stiffness and deflection of a prismatic cantilever, $\bar{y}_{tip} \equiv y_{tip}/y_0$, and (b) and (c) two images of the rib-stiffened cantilever sets under the action of 29 g tip-masses.

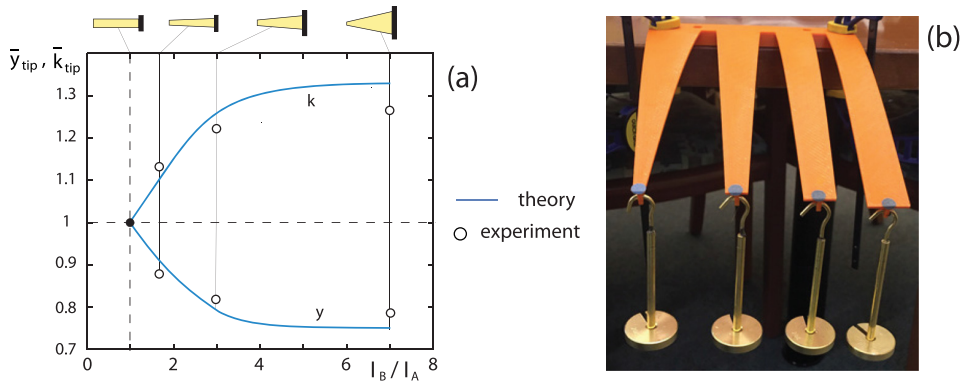

Fig. 6. (a) The effect of varying the taper on the deflection/stiffness of a cantilever, $\bar{y}_{tip} \equiv y_{tip}/y_0$, and (b) image of the tapered cantilevers under the action of 29 g tip masses.

and strain,[19] which, for the four cases considered ($I_B/I_A = 1.0, 1.67, 3, 7$), provides relative tip deflections of 1.0, 0.919, 0.846, and 0.752, and these are shown in Fig. 6 where the relations are evaluated numerically at the given values and then subject to a curve fit. The deflections for these four geometries represent a fairly modest change in tip deflection. However, the volumes (and hence mass) of each of these cantilevers are the same, and thus, the more tapered cantilever may represent a more economic design, at least for this specific (tip-loaded) case. The theory also holds for the (much less practical) case of $I_B/I_A < 1$, in which case the effect is more noticeable, although not included as an example here. A cantilever with a taper in depth also presents certain stiffness benefits. There may be nonstiffness reasons for preferring a tapered cantilever, and the linear theory is less appropriate for more extreme tapers and cases in which the behavior is more plate-like, requiring a more appropriate two-dimensional analysis.[19]

VI. CANTILEVERS WITH A TURNAROUND

A final instructive extension to the deflection behavior of the cantilever can also be achieved using 3D-printing. Consider the situation shown in Fig. 2(c). The end of the cantilever has a "turnaround" attached to it, of length a. If we again subject the system to a lateral point load F, (but now applied to the tip of the turnaround), we find some interesting shapes (and stiffness) depending on the ratio a/L. We ignore the (small) dimensions of the turnaround corner. The governing equation now includes an additional bending moment Fa, located at the main cantilever tip and is given by

$$EI\frac{d^2y}{dx^2} = -F(x-a), \tag{5}$$

where we essentially have a force and a moment at the end of the main cantilever, and these tend to act against each other. Applying the clamped-end boundary conditions, we find the solution

$$y = \frac{FL^3}{3EI}\left[-1 + \frac{3}{2}\left(\frac{x}{L}\right) - \frac{1}{2}\left(\frac{x}{L}\right)^3 + \frac{3}{2}\left(\frac{a}{L}\right)\left(1 - 2\left(\frac{x}{L}\right) + \left(\frac{x}{L}\right)^2\right)\right]. \tag{6}$$

With $a/L = 0$, we obtain the baseline case. However, with $a/L \neq 0$, we see that the deflected shape is not obvious (with something of a trade-off between the bending moments), but again we print a set of similar systems with representative variation in a/L: 1/6, 1/3, 1/2, 2/3, and 5/6. The deflected shapes for these cases are plotted, in Fig. 7(a), for a fixed end load ($FL^2/EI = 0.5566$). Clearly, an interesting question presents itself: what is the tip deflection as a function of a/L?

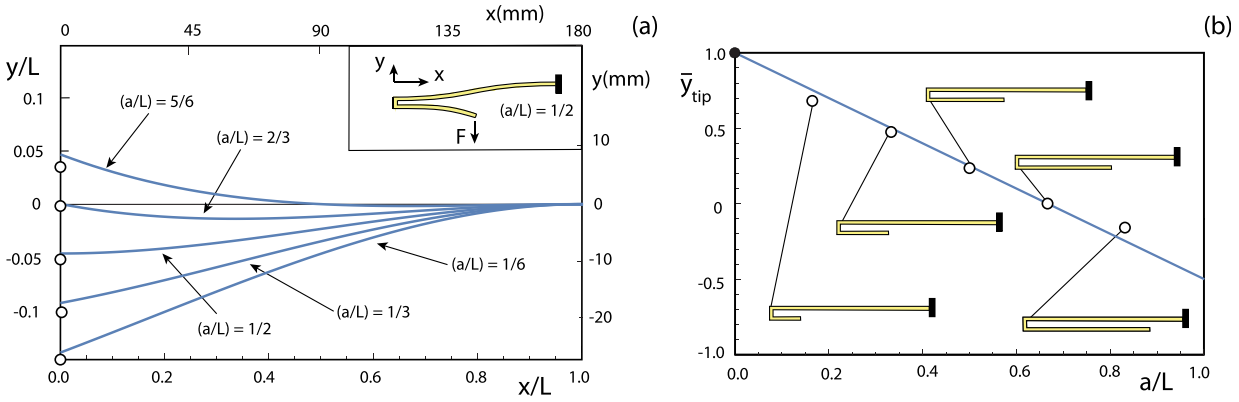

Fig. 7. (a) The deflected shape of a cantilever with various lengths of turnaround, with a sample shape in the inset, axes in the dimensional form included and (b) tip deflection as a function of turnaround length. $\bar{y}_{tip} = y_{tip}/y_{tip,a/L=0}$.

Fig. 8. Three views of a cantilever set with various turnaround lengths under the action of 29 g masses applied at the turnaround tip.

Solving for $y(a/L) = 0$ at $x = 0$ gives $a/L = 2/3$, regardless of the magnitude of F. Also, we see that the case of $a/L = 1/2$ gives a zero slope at the tip (shown in the inset). The tip deflection $\bar{y}_{tip}$ is plotted as a function of turnaround length a/L in Fig. 7(b). Note that the turnaround itself deflects like a cantilever (with typically a nonzero slope and deflection at the attached end), in which the slope of the force vs lateral deflection at the end of the turnaround can be viewed as a stiffness, but the turnaround is used here merely as an easily varied mechanism for influencing the behavior of the main cantilever. Application of linear theory is somewhat restricted in this case, with a more sophisticated analysis indicating a relatively limited range of force for which the tip deflection is positive: it is clear that a relatively large load would inevitably result in a negative tip deflection (despite what the linear theory might say), and again self-weight, which is a little greater for a system with a turnaround, may need to be included (Fig. 8).

VII. CONCLUDING REMARKS

This paper introduces the notion of using sets of 3D-printed cantilevers to provide a tactile demonstration of stiffness and how it is influenced by changes in geometry. Although the measured results are included, this is done mainly for completeness, with the primary emphasis based on relative behavior in which students directly experience the feel of changes in geometry. By simply pushing down on the ends of each cantilever in succession, the change in stiffness is immediately apparent. The focus on relative behavior is intimately related to nondimensionalization and generally de-emphasizes the importance of units. Students can estimate the proportional magnitude of changes in deflection and stiffness as a function of changes in beam geometry.

The resolution of the printer and the material properties of the 3D-printer thermoplastic are much less important than if they were being used to confirm theory against experiment in a conventional sense. 3D-printing is now ubiquitous in science and engineering. We also mention a couple of subtle practical ways in which 3D-printing also facilitates testing: the judicious use of "fillets" on interior corners to reduce stress concentrations; small "eyes" to facilitate the applications of loads (most clearly seen in Fig. 5(b)); and holes printed in the base to allow a convenient attachment to a test-stand.

As mentioned earlier, ABS thermoplastic does not have precise mechanical properties but rather a range, e.g., $1010 < \rho < 1210$ kg/m^3 and $1.2 < E < 2.9$ N/m^2. These are bulk estimates and the 3D-printing process can lead to small voids with different density settings. Furthermore, the nominal values for geometry as printed depend on the resolution of the printer. The deflections are also measured on the top surface of the cantilever whereas the theory corresponds to the cantilever centerline. Thus, we should not be surprised by an imperfect theory-experiment correlation. However, this reinforces the presentation in comparative terms—the cantilevers are all printed with the same material, in the same orientation, into a contiguous base, and to the same geometric tolerance, and hence their relative stiffness/frequency behavior is consistent (as confirmed in the Appendix A).

The (linear) relation between force and deflection is a dominant issue in understanding the mechanics of solids. The advent of 3D-printing presents an appealing opportunity to produce demonstration models that provide an effective (literally) hands-on appreciation of behavior well-supported by fundamental theory.

ACKNOWLEDGMENTS

This work was partially supported by the NSF under Award No. CMMI-1926672. The authors thank the reviewers for their constructive comments.

APPENDIX A: DETAILED MEASUREMENT OF AN INDIVIDUAL CANTILEVER

Since this paper involves producing physical specimens, it is easy enough to take measurements with relatively rudimentary equipment. Stiffness, the slope of the force-deflection relation, is typically measured by taking a set of deflection measurements under different levels of force, and fitting the data using least squares. For the tip-loaded cantilever, measuring force and deflection is straightforward, especially where they are co-located. Either by using a cell load pushing on the end of the cantilever or simply hanging a weight ($F = mg$), the corresponding measured end deflection can be achieved using a proximity laser (an OPTO NCDT 1302 with a precision of 0.025 mm was used in this study). The latter is especially convenient since it does not contact the cantilever and can be aimed to measure deflection at any location. An example is shown in Fig. 9(a). Two cantilevers were subject to increasing levels of tip force. The cantilevers had identical cross sections (25.4×2.5) mm, made from the

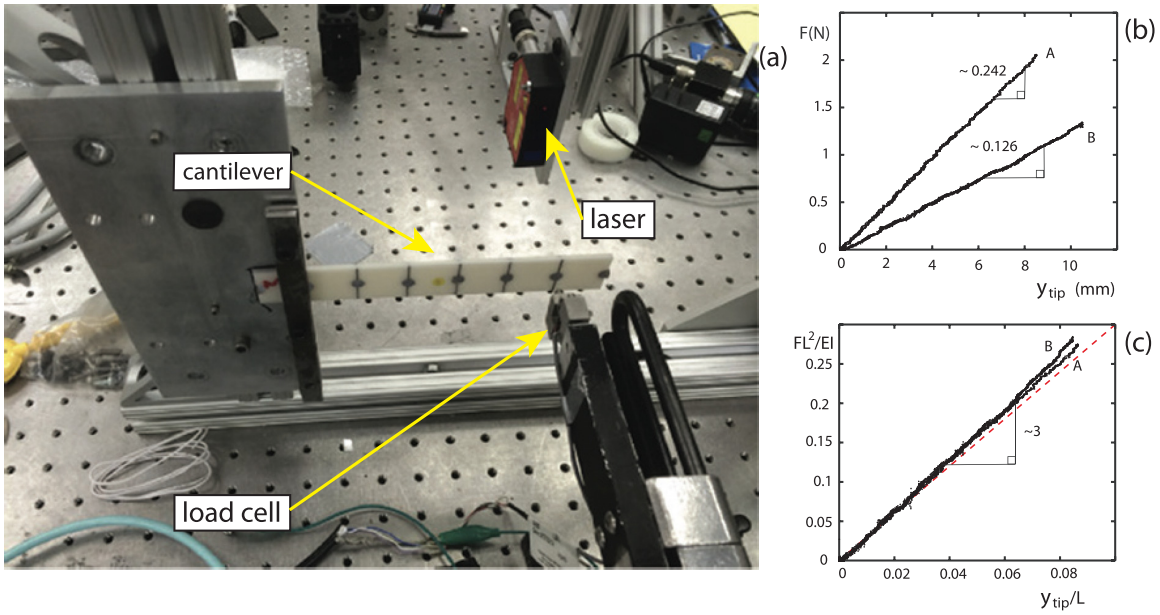

Fig. 9. (a) A 3D-printed cantilever in a test configuration. Under increasing end-load F produced by a displacement-controlled load-cell, the cantilevers bends, with the tip deflection measured using a laser. (b) Dimensional results plotting force (in Newtons) vs deflection (in mm) for two cantilevers of different lengths, and (c) the same data plotted in the dimensionless form, with theory suggesting a slope of 3.

same material (and printed in the same orientation), with the only difference in the length: cantilever A has a length of $L = 98.6$ mm and for cantilever B, $L = 124$ mm.

The experimental data (tip force vs deflection) are shown in Fig. 9(b). In each case, the deflection was measured under increasing and decreasing force using a load cell (an 5-lbf Omega Dyne stainless steel S beam was used in this study), and then repeated, hence the slight spread in the data (in addition to a little electronic noise associated with the measurement devices). A least squares curve fit gave a stiffness (slope) of 0.242 N/mm for cantilever A and 0.126 N/mm for cantilever B. Given the ratio between their lengths ($124/98.6 = 1.254$) and the inverse cubic relation, we would expect all other things being equal, cantilever A to be about $1.254^3 = 1.97$ times stiffer than cantilever B (comparing the slopes in Fig. 9(a) confirms this). Given a deflection for the "unloaded" state ($F = y_{tip} = 0$), the stiffness can be extracted using a single weight and single deflection, as effectively done earlier in this paper. While this is useful in the comparative examples provided in the main body of this paper, a conventional theory vs experimental data study benefits from a more thorough statistical treatment to reduce precision error.

It is instructive to consider these results in nondimensional terms. This provides a convenient basis for comparison, as shown in Fig. 9(c). Here, the axes are FL^2/EI and y_{tip}/L, and we obtain a universal plot in which the slope is close to the theoretical prediction of three. A slight deviation from linearity can be observed for higher loads/deflections, a reminder that the linear theory relies on limiting restrictions.

APPENDIX B: NATURAL FREQUENCIES OF VIBRATION

These types of slender structures are also well-suited for vibration studies, both in terms of a visual appreciation and actual measurements. When disturbed from equilibrium and set into motion, these lightly damped slender elements vibrate in a characteristic fundamental mode of vibration, the

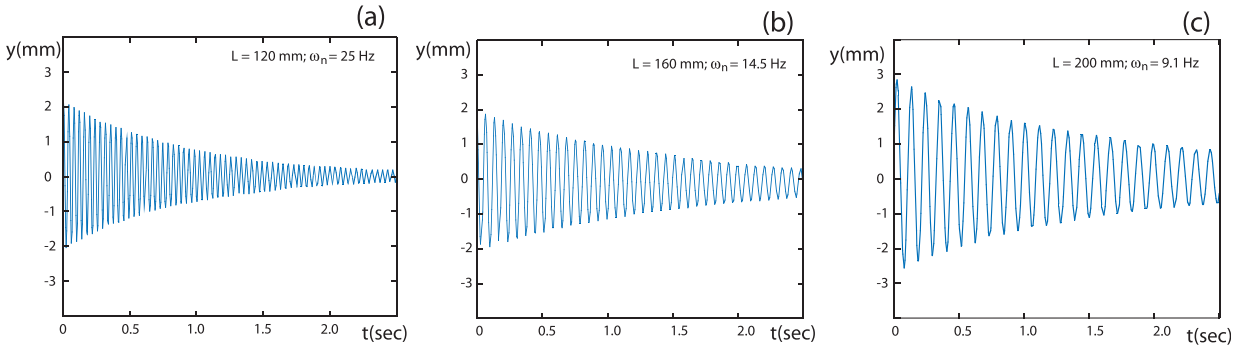

Fig. 10. Time series taken from the standard cantilever with varying length using the same proximity laser as for the static measurement, after the application of a tip displacement and release. (a) $L = 120$ mm, (b) $L = 160$ mm, and (c) $L = 200$ mm.

frequency of which can be related to simple geometry in much the same way as stiffness.

We briefly show some measured frequencies, data acquired with the same proximity laser (with a sampling rate of 750 Hz) as used for the deflection measurements. Figure 10 shows three sample time series, resulting from a sudden tip disturbance. The frequency is extracted using the Fast Fourier Transform (FFT), or by simply counting the number of oscillations over a given time duration. We also see the relatively light damping present in these systems. These oscillations decay exponentially, and we clearly see how the frequency changes with length. Some theoretical and measured frequencies are included in Table II.

A theoretical analysis of the vibration of the cantilever is also a standard exercise in the mechanics of deformable solids. For a prismatic cantilever, it can be shown (based on Euler–Bernoulli theory) that the fundamental natural frequency in bending depends on the geometry and boundary conditions[20–23,25]

$$\omega_n = \frac{3.516}{2\pi L^2}\sqrt{\frac{EI}{m}} = 0.162\left(\frac{d}{L^2}\right)\sqrt{\frac{E}{\rho}}. \tag{B1}$$

We see that the natural frequency scales linearly with the thickness d, and with the inverse square of the length L, so just taking the standard cantilever as an example and comparing cantilevers of different lengths (from Appendix A), we find $\omega_n/\omega_0 = 2.25, 1.65, 1.27,$ and $1, 0.81,$ different ratios that can be readily appreciated from a single pluck. Equation (B1) suggests for the given lengths used in Fig. 10, we would expect the frequencies to be in the ratio 1/0.56/0.36, and indeed the measured values scale as 1/0.58/0.36. It is interesting to observe that changing the width has no effect on the natural frequency (since mass and stiffness are influenced equally), again an effect that can be directly observed from the cantilever set with different widths. Finally, the density of 3D-printing is typically a user-prescribed setting but it is simple enough to weigh specimens if needed.[24]

APPENDIX C: TIP MEASUREMENTS OF THE CANTILEVER SETS

In the measurements of the cantilever sets, the load is applied in a vertical downwards direction (with weights, typically 29 g) and the corresponding deflections are (generally) vertically down and hence negative. A digital load cell is an alternative method of loading, with the advantage of not being restricted to a vertical downward direction and easily incremented. The deflections were measured using a noncontacting laser sensor (the signal is improved using reflective tape—with the small gray targets being apparent in the images of the cantilever sets). The nondimensional normalized stiffnesses and deflections are inverse to each other. The information provided in the following tables was used to populate Figs. 3–7. Theoretical results are based for example on Eq. (3) for Table II and Eq. (6) for Table III, and shown as continuous lines in the figures (with the measured values as the circular symbols). For the values listed in the table below, the data are presented relative to the standard cantilever case, and appear in boldface (Tables IV–VI). Note that the standard case values are typically slightly different in each set due to a small amount of experimental uncertainty

Table II. Influence of changing cantilever length L on deflection y and stiffness k. Theory: $k_0 = 8.54$ N/m; $y_0 = -33$ mm; $\omega_0 = 11.9$ Hz. Measured: $k_0 = 7.37$ N/m; $y_0 = -38.6$ mm; $\omega_0 = 11.3$ Hz. $F = mg = 0.285$ N.

L(mm) (L/L_0)	120 (0.667)	140 (0.778)	160 (0.889)	**180 (1)**	200 (1.111)
k/k_0 (Theory)	3.375	2.125	1.424	**1**	0.729
k/k_0 (Measured)	3.37	2.13	1.42	**1**	0.75
y/y_0 (Theory)	0.296	0.471	0.702	**1**	1.372
y/y_0 (Measured)	0.29	0.46	0.70	**1**	1.34
ω/ω_0 (Theory)	2.25	1.65	1.27	**1**	0.81
ω/ω_0 (Measured)	2.22	1.72	1.28	**1**	0.81

Table III. Influence of changing cantilever width b on deflection y and stiffness k. Theory: $k_0 = 8.54$ N/m; $y_0 = -33$ mm. Measured: $k_0 = 7.37$ N/m; $y_0 = -38.6$ mm. $F = \mathrm{mg} = 0.285$ N.

b (mm) (b/b_0)	10 (0.5)	15 (0.75)	**20 (1)**	25 (1.25)	30 (1.5)
k/k_0 (Theory)	0.5	0.75	**1**	1.25	1.5
k/k_0 (Measured)	0.58	0.79	**1**	1.27	1.42
y/y_0 (Theory)	2	1.333	**1**	0.8	0.667
y/y_0 (Measured)	1.73	1.27	**1**	0.78	0.70

Table IV. Influence of changing cantilever cross section rib-height D on deflection y and stiffness k. Theory: $k_0 = 8.45$ N/m; $y_0 = -33$ mm. Measured: $k_0 = 7.16$ N/m; $y_0 = -39.8$ mm. $F = mg = 0.285$ N.

D (mm)	**0**	1	2	3	4
$k/(k_0(D=0))$ (Theory)	**1**	1.45	2.70	5.10	8.95
k/k_0 (Measured)	**1**	1.52	3.06	5.77	10.76
y/y_0 (Theory)	**1**	0.69	0.37	0.20	0.11
y/y_0 (Measured)	**1**	0.66	0.33	0.17	0.09

Table V. Influence of changing cantilever taper on deflection y and stiffness k. Theory: $k_0 = 8.54$ N/m; $y_0 = -33$ mm. Measured: $k_0 = 7.26$ N/m; $y_0 = -39.2$ mm. $F = mg = 0.285$ N.

b_A, b_B (mm)	**20, 20**	15, 25	10, 30	5, 35
I_B/I_A	**1**	1.67	3	7
k/k_0 (Theory)	**1**	1.09	1.26	1.33
k/k_0 (Measured)	**1**	1.13	1.22	1.26
y/y_0 (Theory)	**1**	0.92	0.79	0.75
y/y_0 (Measured)	**1**	0.88	0.82	0.79

Table VI. Influence of changing cantilever end turnaround length a on end deflection y. $L_0 = 180$ mm. Theory: $y_{tip}(a=0) = -33$ mm. Measured: $y_{tip}(a=0) = -39$ mm (from a previous set). $F = mg = 0.285$ N.

a (mm) (a/L_0)	**0 (0)**	30 (0.167)	60 (0.333)	90 (0.5)	120 (0.667)	150 (0.833)
y_{tip}/y_0 (Theory)	**1**	0.75	0.5	0.25	0	−0.25
y_{tip}/y_0 (Measured)	**1**	0.69	0.48	0.26	0.03	−0.15

and variability. Since the baseline values are divided by themselves, they are included as black data points in the figures.

[a)]l.virgin@duke.edu

[1]S. P. Timoshenko, *Strength of Materials* (Van Nostrand, New Jersey, 1977).
[2]H. L. Langhaar, *Dimensional Analysis and the Theory of Models* (Wiley, New York, 1951).
[3]F. M. Lanchester, *The Theory of Dimensions and Its Applications for Engineers* (Crosby-Lockwood, London, 1940).
[4]E. Buckingham, "On physically similar systems: Illustrations of the use of dimensional equations," Phys. Rev. **4**, 345–376 (1914).
[5]L. N. Virgin, "Enhancing the teaching of linear structural analysis using additive manufacturing," Eng. Struct. **150**, 135–142 (2017).
[6]L. D. Peel and M. Abdelrahman, "Studying the physical properties and auxetic behavior of 3D-printed fasteners," in Proceedings of the ASEE Annual Conference (2012).
[7]S. S.-H. Kim, "Development of a laboratory module in 3D printing," in ASEE Annual Conference, Paper No. 17818 (2017).
[8]J. Wang, N. C. Golly, B. Herren, J. I. MacDonald, Z. Siddique, and Y. Liu, "Enhancing mechanical engineering education with an integrated 3D printing approach," in ASEE Annual Conference (2019).
[9]L. N. Virgin, "On the flexural stiffness of 3D printer thermoplastic," Int. J. Mech. Eng. Educ. **45**, 59–75 (2017).
[10]I. M. Alhamad, W. K. Ahmed, H. Z. Ali, and H. AlJassmi, "3D printing applications in mechanical engineering education," *Integrating 3D Printing into Teaching and Learning* (Brill Sense, Leiden, 2019), pp. 90–131.
[11]S. Ford and T. Marshall, "Invited review article: Where and how 3D printing is used in teaching and education," Addit. Manuf. **25**, 131–150 (2019).
[12]R. C. Hibbeler, *Structural Analysis* (Pearson Education, London, 2008).
[13]K. A. Peska II, "Interdisciplinary cantilever physics: Elasticity of carrot, celery, and plasticware," Am. J. Phys. **82**, 484–489 (2014).
[14]F. Wilson and A. E. Lord, Jr., "Young's modulus determination via simple, inexpensive static and dynamic measurements," Am. J. Phys. **41**, 653–656 (1973).
[15]J. R. Taylor, *An Introduction to Uncertainty Analysis: The Study of Uncertainties in Physical Measurements* (University Science Books, Mill Valley, 1982).
[16]H. D. Young, *Statistical Treatment of Experimental Data* (McGraw-Hill, New York, 1962).
[17]L. N. Virgin, "Sympathetic resonance," Am. J. Phys. **86**, 439–442 (2018).
[18]W. D. Pilkey, *Analysis and Design of Elastic Beams* (John Wiley and Sons, New York, 2002).
[19]W. C. Young, R. G. Budynas, and A. M. Sadegh, *Roark's Formulas for Stress and Strain*, 8th ed. (McGraw-Hill, New York, 2012).
[20]R. D. Blevins, *Formulas for Natural Frequency and Mode Shape* (Krieger Publishing Company, Florida, 1979).
[21]W. T. Thomson, *Theory of Vibration with Applications* (Prentice-Hall, Englewood Cliffs, NJ, 1981).
[22]K. Turvey, "An undergraduate experiment on the vibration of a cantilever and its application to the determination of Young's modulus," Am. J. Phys. **58**, 483–487 (1990).
[23]S. Velasco, F. L. Roman, and J. A. White, "A simple experiment for measuring bar longitudinal and flexural vibration frequencies," Am. J. Phys. **78**, 1429–1432 (2010).
[24]J. H. Porter, T. M. Cain, S. L. Fox, and P. S. Harvey, "Influence of infill properties on flexural rigidity of 3D-printed structural members," Virtual Phys. Prototyping **14**, 148–159 (2019).
[25]L. N. Virgin, *Vibration of Axially Loaded Structures* (Cambridge U. P., New York, 2007).

Lens Set for Eye Testing

This set of concave and convex test lenses must have been given to the physics department at Hobart and William Smith Colleges by a local Geneva, New York, optician in the mid-20th century. The power of the lenses goes up and down in steps of 0.25 diopters. As optical testing moves to more sophisticated methods, these sets become available. I have found them quite useful in lecture demonstrations and in one-on-one laboratory teaching. (Picture and text by Thomas B. Greenslade, Jr., Kenyon College)